Multidimensional Noise Reduction in C-arm Cone-beam CT via 2D-based Landweber Iteration and 3D-based Deep Neural Networks

Dahim Choi[1], Juhee Kim[2], Seung-Hoon Chae[3], Byeongjoon Kim[4], Jongduk Baek[4], Andreas Maier[5], Rebecca Fahrig[6], Hyun-Seok Park[1], Jang-Hwan Choi[2]

[1] Computer Science and Engineering, Ewha Womans University, Seoul 03760, Korea;
[2] Division of Mechanical and Biomedical Engineering, Ewha Womans University, Seoul 03760, Korea;
[3] Electronics and Telecommunications Research Institute, Daejeon 34129, Korea;
[4] School of Integrated Technology, Yonsei University, Incheon 406840, Korea;
[5] Friedrich-Alexander University Erlangen-Nuremberg, Erlangen 91058, Germany; [6] Siemens Healthcare GmbH, Erlangen 91052, Germany

ABSTRACT

Recently, the necessity of using low-dose CT imaging with reduced noise has come to the forefront due to the risks involved in radiation. In order to acquire a high-resolution image from a low-resolution image which produces a relatively small amount of radiation, various algorithms including deep learning-based methods have been proposed. However, the current techniques have shown limited performance, especially with regard to losing fine details and blurring high-frequency edges. To enhance the previously suggested 2D patch-based denoising model, we have suggested the 3D block-based REDCNN model, employing convolution layers paired with deconvolution layers, shortcuts, and residual mappings. This process allows us to preserve the image structure and diagnostic features of an image, increasing image resolution by smoothing noise. Finally, we applied a bilateral filter in 3D and utilized a 2D-based Landweber iteration method to reduce remaining noise under a certain amplitude and prevent the edges from blurring. As a result, our proposed method effectively reduced Poisson noise level without losing diagnostic features and showed high performance in both qualitative and quantitative evaluation methods compared to ResNet2D, ResNet3D, REDCNN2D, and REDCNN3D.

Keywords: deep neural networks, noise reduction, imaging of lower extremities, C-arm cone-beam CT, Landweber type iteration, bilateral filtering, medical image processing

1. INTRODUCTION

The use of CT for diagnosis has increased rapidly and widely, and some patients in high-risk situations now need repeated scans to monitor their conditions. Meanwhile, as the deleterious effects of exposure to radiation have been uncovered, the potential risks of radiation have been brought to common awareness. One way to reduce radiation exposure to patients is to lower the dose of radiation administered in each CT scan. However, lowering the radiation dose increases noise in the image and degrades image quality, which negatively affects the practitioner's ability to make an accurate diagnosis. Therefore, developing methods to obtain diagnostic-quality images from low-dose CT scans by implementing noise reduction techniques has become an undisputed necessity.

To suppress noise in low-dose CT imaging, some state-of-the-art techniques utilizing Convolutional Neural Networks (CNN) including ResNet [1] and REDCNN [2] have been suggested [1, 3-7]. Image denoising methods based on deep learning have shown improved performance compared to conventional denoising algorithms such as BM3D [8], wavelet thresholding [9], wavelet multi-frame denoising [10], and Bayesian estimation denoising [11]. However, denoising with CNN architectures has the tendency to lose fine image details and blur out high-frequency edges. This is because the accumulated loss is not suitable for image reconstruction when the network goes deeper. In addition, when the network depth increases, the gradient diffusion makes the network difficult to train [2]. ResNet and REDCNN tried to overcome these problems by utilizing residual mapping.

To further improve image quality, our research team proposed a multidimensional noise reduction algorithm in C-arm Cone-beam CT. We hypothesized that 3D block-based architectures may perform better than 2D patch-based architectures because the adjacent image slices in a CT volume have strong correlative features [12]. Therefore, we intended to improve performance by modifying the previously suggested 2D networks into 3D. Moreover, we applied a 3D bilateral filter and a 2D-based one-step Landweber-type iteration. In the research described in this paper, we have implemented ResNet and REDCNN in both patch-based and block-based models, and have compared the results with our proposed model.

2. MATERIALS AND METHODS

2.1 Patient data acquisition

Under an IRB-approved protocol, 18 volunteers were imaged while lying supine using two different C-arm cone-beam CT systems (Artis Zeego and Axiom Artis dTA, Siemens Healthcare GmbH, Forchheim, Germany) with a flat panel detector. The detector produced a matrix of 1240×960 pixels with 0.308 mm isotropic resolution after 2×2 binning. The acquisition protocol used the minimum allowed value of the kVp of 70, a detector dose request of 1.2 µGy/frame, and 496 frames over π plus fan angle in 20 seconds. Projection-specific values of mAs and kV were modulated by a built-in automatic exposure control system [13]. The projection images were reconstructed in a 32-bit depth volumetric image of 512 voxels with an isotropic spacing of 0.5 mm using filtered back projection (FBP) using CONRAD [14]. The forward and backward projection processes were GPU-accelerated [15].

2.2 Multidimensional noise reduction process

2.2.1 Noise reduction in 3D via CNN with 3D kernels

REDCNN consists of encoder and decoder layers [2]. In encoder layers, there are two types of layers: convolutional layers and ReLU units. Similarly, decoder layers have transposed convolutional layers and ReLU units. Since the encoder and decoder should match up, REDCNN is composed of the same number of convolutional and deconvolutional layers. The network has shortcuts which connect the matching convolutional and deconvolutional layers, and both layers have the same kernel size. We used a 3×3×3 kernel size and a 32×32×32 block size, measured in pixels. Figure 1 shows that the patches went into the network featuring the symmetry of paired convolution and deconvolution layers. The L_2 loss function was optimized by Adam [2]. The two subjects' volumetric images were used as a test dataset to unbiasedly evaluate a final CNN model fit on the training dataset. The noisy low-dose images paired with the high-dose FBP-reconstructed images were generated by imposing Poisson noise into each voxel.

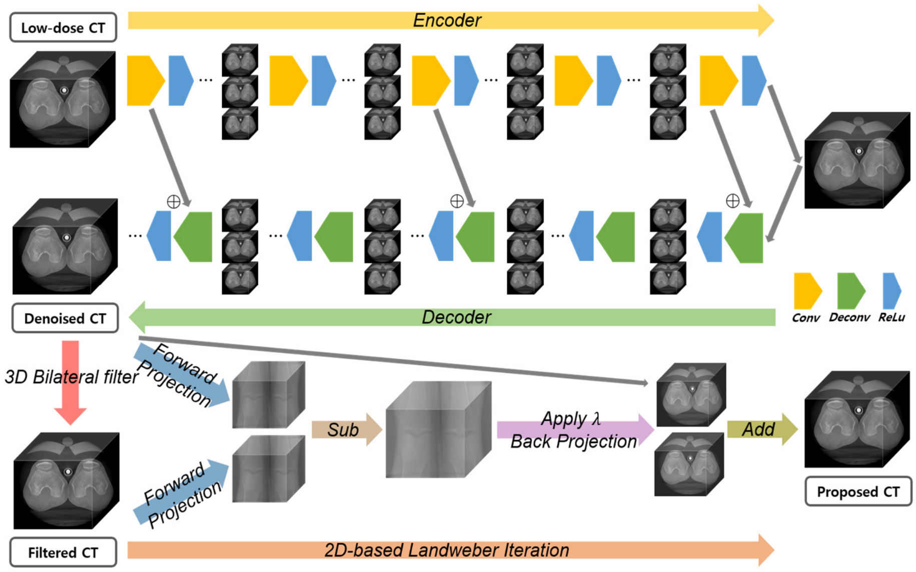

Figure 1.

Multidimensional noise reduction process. First, 3D blocks of low-dose CT imaging are sent through the REDCNN3D model. Then, the reconstructed outcome is filtered by a bilateral filter in 3D. With forward projection, the 2D result of denoised CT and filtered CT can be compared, and the difference contains information that we want to reduce or retain.

2.2.2 Noise reduction in 2D via a Landweber-type iteration

Although the REDCNN3D network showed outstanding performance in Poisson noise reduction, reducing noise through the CNN network has the drawback of blurring the edges. In medical imaging, the edge is crucial for diagnosis because it contains information about lesions. Therefore, to deal with the edge-blurring problem and to smooth the remaining noise, we applied a bilateral filter to image voxel vector x^1, an outcome of the REDCNN3D network. Using a non-linear, bilateral filter allowed us to preserve the border line and decrease the Poisson noise level. Based on spatial distance (σ_s) and radiometric differences (σ_r), the filter smoothed noise below a certain intensity of amplitude. The radiometric differences (σ_r) used in our method were determined by the intensity interval between fat and muscle, the minimum we want to conserve. Finally, we utilized the FDK algorithm [16] to create a 3D bilateral filtered image, thus implementing a Landweber-type reconstruction in one step [17]. The performance of the combination of bilateral filtering and Landweber iterations was similar with that of a total variation regularized iterative reconstruction [18], and the cost associated with the combination was relatively low.

The whole process is described as follows: 1) Acquire REDCNN3D applied reconstruction CT image (x^1). 2) Apply a 3D bilateral filter on voxel vector x^1 with σ_s and σ_r. 3) Implement one step Landweber-type reconstruction using the following FDK algorithm: $x^2 = x^1 + \lambda A^T(b - Ax^1)$, where A is a forward-projector, A^T is a backward-projector, λ is a step size, and b is projected data in 2D. In this study, λ was determined as 0.7 heuristically.

2.3 Measurement of noise reduction and the line profile

In order to assess the performance of each method, we measured the structural similarity index (SSIM) and noise level (% standard deviation) between a low-dose image (x^0) and an outcome reconstructed image (x^2). Generally, SSIM is used to evaluate the similarity between two images and is designed to improve on traditional metrics such as peak-signal-to noise ratio (PSNR) and mean squared error (MSE) [19]. The closer the index is to 1, the better the performance of the model. We calculated the SSIM over the whole region of reference in the testing images, including the standard deviation over the space between the legs. We also measured the intensity across the border between fat and muscle, and the boundary between cortical bone and fat, as indicated by the arrows in Fig. 3(a).

3. RESULTS

3.1 Qualitative evaluation

Representative reconstructed slices of the test dataset of two healthy subjects are displayed in Fig. 2. In this study, the main causes of the low-frequency background noise in the low-dose images were found to be the Poisson noise imposed and limitations of a standard FBP reconstruction. As the arrows in the low-dose images (a4 and a5) indicate, severe background noise appeared like a white band especially around the central region in the sagittal plane which degraded soft tissue visibility. Between REDCNN3D (e5) and ResNet3D (c5), REDCNN3D reduced the background noise better. When comparing the performance of 2D and 3D models, REDCNN3D (e5) better suppressed the noise than REDCNN2D (d5). Among all the methods tested, the proposed method (f5) showed the best performance, suppressing the noise almost completely to the noise level in the reference image (g5). As the arrows in e3 and f3 indicate, streak artifacts and the background noise present in REDCNN3D were effectively suppressed when using the proposed method. The pattern of the performance difference of the method mentioned above was relatively clear in the fourth and fifth rows (a-g4 and a-g5) of a sagittal plane, but similar patterns were found in other rows.

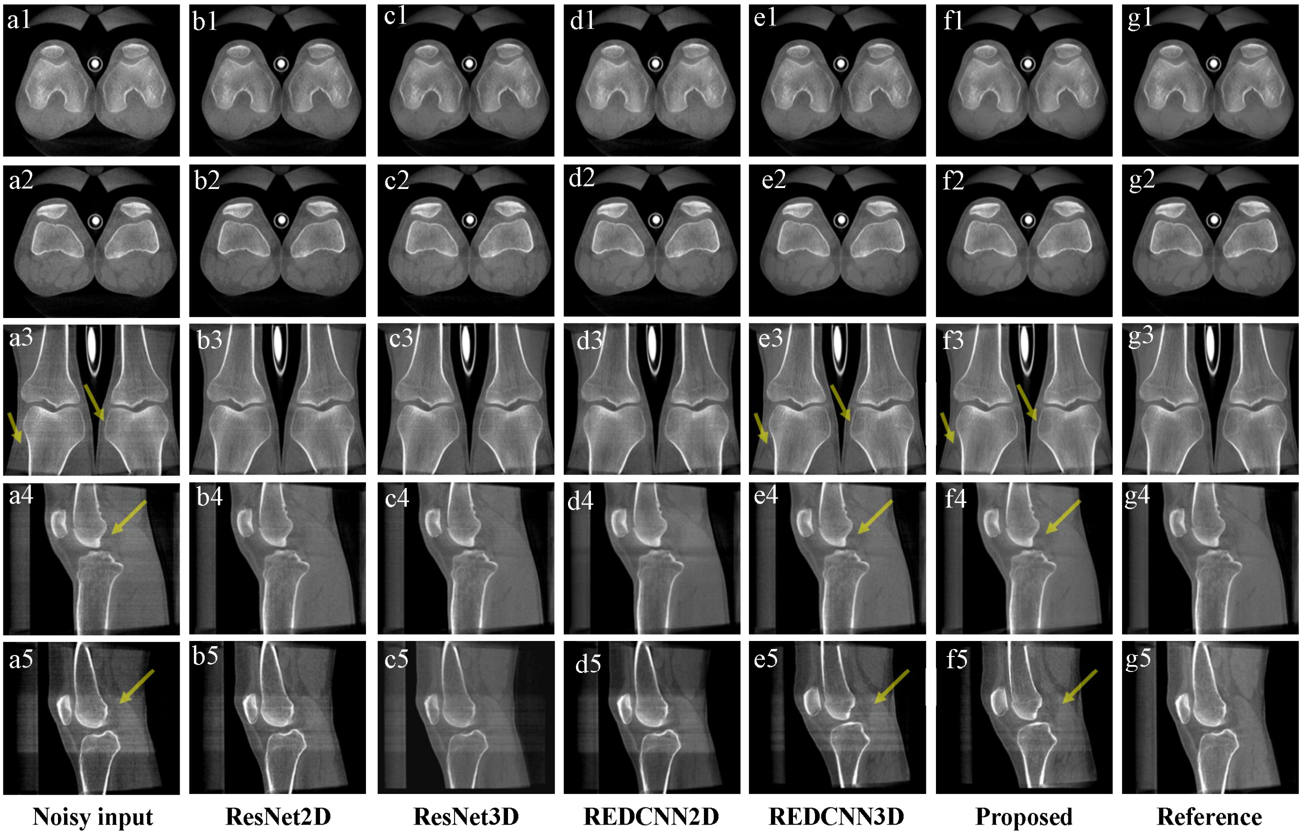

Figure 2. The left and rightmost columns in the figure show the noisy low-dose input (a) and reference (g), respectively. The remaining columns correspond to images processed with ResNet2D (b), ResNet3D (c), REDCNN2D (d), REDCNN3D (e), and the proposed method (f). To better appreciate the differences in image quality, it is recommended to magnify the images as much as possible.

3.2 Quantitative evaluation

Representative line profiles of the low and high contrast edges are shown in Fig. 3, and they were extracted from the same subject data as in Fig. 2. The current state-of-the-art denoising method, REDCNN2D, was not capable of recovering edges with low contrast well, as seen with its line profiles showing the noise-like fluctuation and the Hounsfield unit (HU) values of fat that did not decrease even after passing through the muscle-fat edge (see Fig. 2[b]). In contrast, the line profiles of 3D block-based REDCNN3D confirmed that in this method, edges with low contrast were reconstructed well without degrading spatial resolution. As seen in Fig. 3(b-c), the proposed method achieved even sharper line profiles over both the weak and strong edges by reducing artifacts and noise in the uniform area of low density material (fat), indicated by the magnitude of the first peaks on the right side of the solid vertical line.

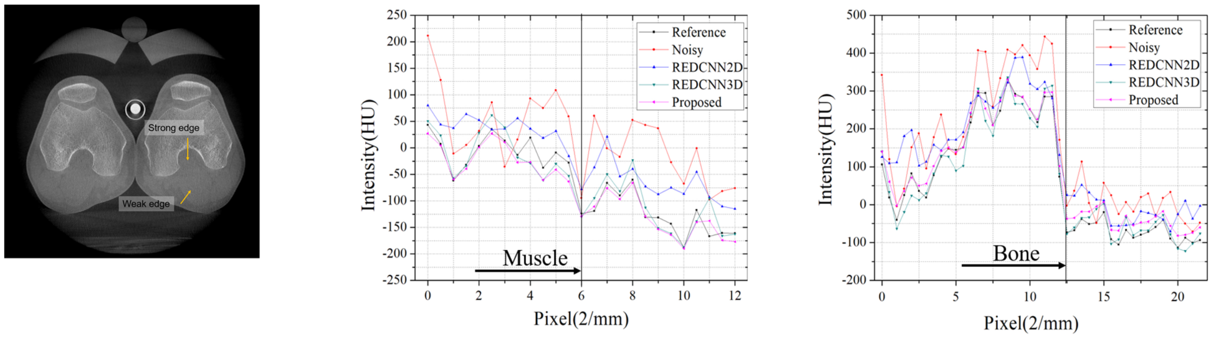

(a) Region of interest (ROI) for line profiles in (b) and (c)

(b) Line profiles over the weak edge in (a)

(c) Line profiles over the strong edge in (a)

Figure 3. Comparison among the line profiles of noisy input, reference, and images processed with three correction methods over the weak edge and strong edge marked on (a). (a) Line profiles ROI in central slice. (b) The line profiles of the weak edge across muscle and fat. (c) The line profiles of the strong edge across bone and fat.

As observed qualitatively, the proposed method showed the best performance, achieving the highest SSIM (see Table 1). The proposed algorithm suppressed noise by approximately 24% compared with the noisy input image (82% → 58%). This noise reduction was enabled by the edge-preserving property of a bilateral filter preserving edges over the threshold level (σ_r).

	SSIM [0-1]	Noise, σ [HU]
Noisy input (low-dose)	0.7737 (±0.0493)	82.52 (±2.94)
ResNet2D	0.8667 (±0.0027)	72.15 (±3.17)
ResNet3D	0.9233 (±0.0026)	65.58 (±2.70)
REDCNN2D	0.8954 (±0.0019)	58.56 (±2.95)
REDCNN3D	0.9258 (±0.0021)	65.58 (±2.91)
Proposed method	0.9399 (±0.0023)	58.73 (±3.14)

Table 1. Quantitative results in terms of image quality (the SSIM) and the background noise (the standard deviation [σ] of the background intensity) in HU. The results are associated with different algorithms.

4. CONCLUSIONS

Denoising with current CNN architectures has the tendency to lose fine image details and blur out a high-frequency edge. In this research, we overcame these problems using the proposed multidimensional noise-reduction algorithm working on both the 2D projection and the 3D image domains incorporating a Landweber-type iteration in 2D and a volumetric block-based CNN architecture in 3D into one step. The newly proposed method suppressed background noise effectively and also reduced streak artifacts while preserving fine spatial resolution. The proposed method showed better performance both qualitatively and quantitatively than current state-of-the-art CNN denoising models including ResNet and REDCNN.

ACKNOWLEDGEMENT

This research was supported by the National Research Foundation of Korea (NRF) grant funded by the Korean government, MSIP (grant no: NRF-2015M3A9A7029725 and NRF-2017M2A2A6A02070522, URL: http://nrf.re.kr). The funders had no role in study design, data collection and analysis, decision to publish, or preparation of the manuscript. This work was never submitted, published, or presented before.

REFERENCES

[1] K. Zhang, W. Zuo, Y. Chen *et al.*, “Beyond a gaussian denoiser: Residual learning of deep cnn for image denoising,” IEEE Transactions on Image Processing*,* 26(7), 3142-3155 (2017).

[2] H. Chen, Y. Zhang, M. K. Kalra *et al.*, “Low-Dose CT With a Residual Encoder-Decoder Convolutional Neural Network,” IEEE Trans Med Imaging*,* 36(12), 2524-2535 (2017).

[3] C. Dong, C. C. Loy, K. He *et al.*, "Learning a deep convolutional network for image super-resolution." 184-199.

[4] L. Gondara, "Medical image denoising using convolutional denoising autoencoders." 241-246.

[5] X. Mao, C. Shen, and Y.-B. Yang, "Image restoration using very deep convolutional encoder-decoder networks with symmetric skip connections." 2802-2810.

[6] T. Würfl, F. C. Ghesu, V. Christlein *et al.*, "Deep learning computed tomography." 432-440.

[7] T. Wurfl, M. Hoffmann, V. Christlein *et al.*, “Deep Learning Computed Tomography: Learning Projection-Domain Weights From Image Domain in Limited Angle Problems,” IEEE Trans Med Imaging*,* 37(6), 1454-1463 (2018).

[8] K. Dabov, A. Foi, V. Katkovnik *et al.*, "BM3D image denoising with shape-adaptive principal component analysis."

[9] F. Luisier, T. Blu, and M. Unser, “A new SURE approach to image denoising: Interscale orthonormal wavelet thresholding,” IEEE Transactions on image processing*,* 16(3), 593-606 (2007).

[10] M. A. Mayer, A. Borsdorf, M. Wagner *et al.*, “Wavelet denoising of multiframe optical coherence tomography data,” Biomedical optics express*,* 3(3), 572-589 (2012).

[11] E. P. Simoncelli, [Bayesian denoising of visual images in the wavelet domain] Springer, (1999).

[12] H. Shan, Y. Zhang, Q. Yang *et al.*, “3D convolutional encoder-decoder network for low-dose CT via transfer learning from a 2D trained network,” arXiv preprint arXiv:1802.05656, (2018).

[13] M. Soderberg, and M. Gunnarsson, “Automatic exposure control in computed tomography--an evaluation of systems from different manufacturers,” Acta Radiol*,* 51(6), 625-34 (2010).

[14] A. Maier, H. G. Hofmann, M. Berger *et al.*, “CONRAD--a software framework for cone-beam imaging in radiology,” Med Phys*,* 40(11), 111914 (2013).

[15] H. Scherl, B. Keck, M. Kowarschik *et al.*, [Fast GPU-based CT reconstruction using the common unified device architecture (CUDA)], (2007).

[16] L. A. Feldkamp, L. C. Davis, and J. W. Kress, “Practical Cone-Beam Algorithm,” Journal of the Optical Society of America a-Optics Image Science and Vision*,* 1(6), 612-619 (1984).

[17] L. Landweber, “An iteration formula for Fredholm integral equations of the first kind,” American journal of mathematics*,* 73(3), 615-624 (1951).

[18] M. T. Manhart, M. Kowarschik, A. Fieselmann *et al.*, “Dynamic iterative reconstruction for interventional 4-D C-arm CT perfusion imaging,” IEEE Trans Med Imaging*,* 32(7), 1336-48 (2013).

[19] A. Hore, and D. Ziou, "Image quality metrics: PSNR vs. SSIM." 2366-2369.